Cluster formation in the adsorbate-induced reconstruction of the O/Mo(001) surface

1992 J. Phys.: Condens. Matter 4 5845

(http://iopscience.iop.org/0953-8984/4/27/003)

J. Phys.: Condens. Matter 4 (1992) 5845–5854. Printed in the UK

Cluster formation in the adsorbate-induced reconstruction of the O/Mo(001) surface

I K Robinson, D-M Smilgies and P J Eng
AT&T Bell Laboratories, Murray Hill, NJ 07974, USA

Received 6 April 1992

Abstract. An x-ray crystallographic structure determination has been carried out for the $\sqrt{5}\times\sqrt{5}$ Mo(001)/O surface. This is the penultimate structure in the sequence of ordered states obtained by high-temperature desorption from the oxidized surface. The oxygen induces a reconstruction with one Mo atom missing from the surface unit cell and O atoms occupying the exposed threefold sites. The O sits asymmetrically in these sites and induces a rotational distortion of the remaining top layer Mo atoms, which cluster together. The asymmetry can be attributed to partial direct bond formation between surface Mo–O clusters, since apparently this is not mediated by any significant second-layer displacements.

Oxygen-induced structures on molybdenum can be viewed as model systems of oxidation precursors for transition metal surfaces in general. Mo has one of the widest ranges of oxides known with a large variation of stoichiometry and crystal structure [1]. Despite the fact that there have been a number of thorough LEED studies of the Mo(001)/O adsorbate system [2–10] over the years, not much more than the symmetry is known of the actual structure of these phases. In this paper we present the first determination of one of the well-ordered O structures. It reveals an unusual asymmetric threefold coordination of the oxygen atoms that is understood to be caused by partial interactions with more distant neighbours.

When a superstructure is observed in an adsorbate/surface chemisorption system, it is usually assumed to arise from partial filling of available substrate sites by the adsorbate atoms. Interactions, usually in the form of delicately balanced attractive and repulsive forces, can be inferred to explain the translational symmetry observed, but it is increasingly difficult to explain some of the high-order structures found or the rich variety seen in some phase diagrams. More recently, however, it has been realised that when substrate diffusion becomes a relevant parameter in reaching the stable configuration, the conservation of complete monolayers of the substrate is no longer a boundary condition for determining a structure. The resulting 'adsorbate-induced reconstruction' can manifest itself in the form of 'adatoms', 'vacancies', 'missing rows' or just as induced substrate displacements. This has by now been seen in a number of systems including O/Cu(110) [11], O/Cu(100) [12] and N/Ni(100) [13], and can be expected to become a common occurrence.

Room temperature adsorption of O on Mo(001) gives a consecutive series of ordered structures, c(2×2), followed by 6×2, then 6×1, then 3×1 and finally 1×1 [6, 8, 9]. On the other hand, high-temperature adsorption (above 1000 K) gives an

0953-8984/92/275845+10$04.50

altogher different series, c(4×4), 2×1, $\sqrt{5}\times\sqrt{5}$, 2×1, c(2×2), and eventually produces facetted structures [2–10]. The formation of these facetted states has been investigated and found to result in oxide layers [5, 7, 10] that start at 1000 L (1 L = 10^{-6} Torr s) and saturate at 5000 L [10]. Thermal desorption from the oxide state yields the high-temperature series of surface structures in reverse order [6–10]. The oxygen coverages corresponding to each state have been determined by careful quantitative Auger spectroscopy measurements [8–10].

In this paper, we report the atomic structure of the $\sqrt{5}\times\sqrt{5}$ phase that occurs at an O coverage of 0.8 monolayers (ML). Of the various high-temperature phases, this one appears to have the widest stability range. It is also the highest coverage chemisorbed phase that is well-ordered, in the sense of having a sharp LEED pattern. All structures with higher coverages are somewhat diffuse in LEED, a fact that has been attributed to the onset of O-induced facetting [5–10] of the surface, followed by three-dimensional oxidation. Our x-ray diffraction study focusses on the structure of the $\sqrt{5}\times\sqrt{5}$ phase in order to gain some insight about this transition from the chemisorption to facetting regimes.

Our experiments have been carried out in an ultra-high vacuum (UHV) chamber at a base pressure of 1×10^{-10} mbar which is equipped with standard surface diagnosis tools: a LEED system and an Auger spectrometer [14]. Oxygen (MG Scientific, purity 99.8%) was dosed into the chamber with a leak valve. The Mo(001) single-crystal sample was oriented and polished commercially [15] and had already been used in a previous experiment [16]. It was found to have a slight miscut of $1.14 \pm 0.1°$ along a direction 18° away from [010] and a mosaic spread of $<0.02°$, as determined by x-ray diffraction. The sample was cleaned by oxidizing it at 1000 K in an oxygen pressure of 1×10^{-7} mbar for 5 min and then flashing to 2200 K by electron bombardment from the back [17]. The $\sqrt{5}\times\sqrt{5}$ structure was prepared following the same procedure except that the sample was flashed only to 1500 K and resulted in a sharp uniform LEED pattern.

X-ray diffraction measurements were performed at beamline X16A at the National Synchrotron Light Source (NSLS), Brookhaven National Laboratory, on a 5-circle diffractometer designed for surface experiments. High stability is achieved by direct coupling of the diffractometer to the sample inside the UHV chamber [14]. Bending magnet radiation was collected and focussed with a toroidal Pt-coated mirror, and a wavelength of 1.78 Å was selected with a double-crystal Si(111) monochromator. The crystal was aligned by means of the bulk [101] and [011] reflections. Crystallographic measurements of observed structure factors were made by integration of 'omega' scans, followed by background subtraction and correction for the Lorentz factor, the polarization factor and the active sample area [18]. An additional out-of-plane area correction was derived for the 5-circle mode and is described in the appendix.

The diffraction pattern was indexed conventionally for body-centred cubic, using the convention that Miller index l is perpendicular to the surface plane. The diffraction from the $\sqrt{5}\times\sqrt{5}$ superstructure of the reconstruction had in-plane indices hk which were multiples of 1/5, while l was a continuous variable. A large in-plane dataset was collected at $l = 0.1$ and a grazing incidence angle of 0.4°. We used the method of Vlieg *et al* [19] for the 5-circle setting calculation. The plane group symmetry of the $\sqrt{5}\times\sqrt{5}$ superstructure is $p4$, since it has no mirror planes. On a substrate with $p4m$ symmetry two possible orientations of the superstructure can arise, called 'twin domains'. No significant difference between the intensities of the two twin domains was detected however. The eight $p4m$ symmetry equivalents of each reflec-

tion, four from each twin domain, were therefore measured and averaged together; the variation among them was used as an error estimate. A total of 29 independent fractional-order and 4 integer-order reflections were collected altogether. 44 hours later some reflections were rechecked and found to have become somewhat *larger* in intensity, but still within the 10% average error estimate. This measurement period was assumed to be the effective sample lifetime at 10^{-10} Torr. A second preparation of the sample was then used to measure the l-dependence of four reflections, this time with four symmetry equivalents each. Here grazing *exit* conditions [19] were used with an exit angle of 2°. The two datasets merged with a scale factor of 1.5, found to match up at the $l = 0.1$ points.

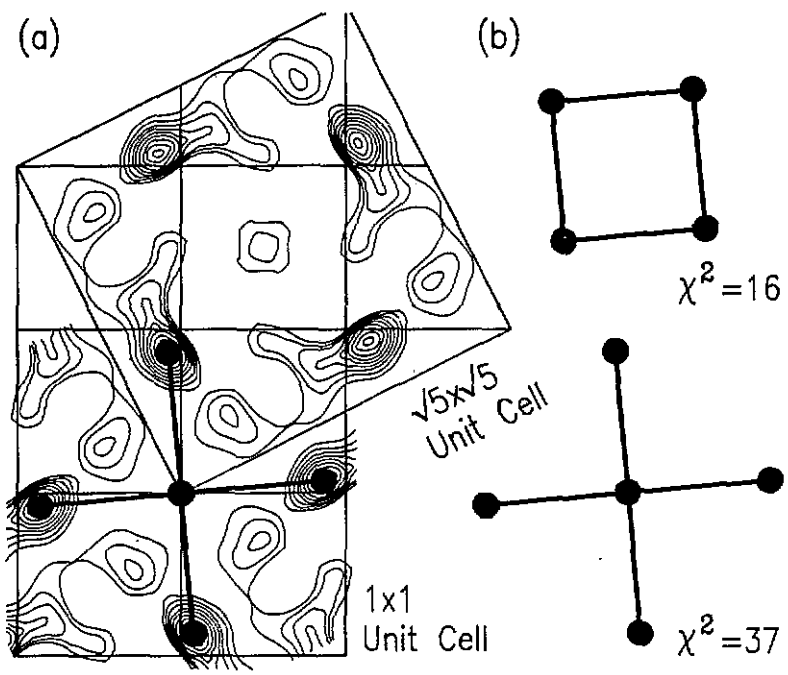

Figure 1. (*a*) Contour map of the Patterson function of the in-plane fractional-order data. The origin peak has been suppressed by subtraction of the average intensity value from each of the input intensities. Only positive contours are shown with equal spacing. The indicated peak identifies the fundamental interatomic vector in the structure. (*b*) Two atomic arrangements consistent with the position of the observed Patterson peak.

The two-dimensional Patterson function for the fractional-order in-plane data is shown in figure 1(*a*). The origin has been suppressed from the plot, as have the peaks that would appear at bulk interatomic vectors, because of the omission of the integer-order data. A single, clear positive peak identifies the principal interatomic vector in the structure, presumably a Mo–Mo vector, since O is a relatively weak scatterer of x-rays. Figure 1(*b*) shows two spatial arrangements of atoms consistent with the Patterson function. A structure factor calculation was then carried out assuming $p4$ plane group symmetry as explained above. Using the models of figure 1(*b*) for starting parameters and allowing two coordinates plus a thermal vibration parameter to vary until they reached optimal values, the calculation gave the χ^2 values indicated. Clearly the 4-atom structure is the correct choice. The secondary peaks of the

Patterson function and a Fourier difference map [18] were used to identify potential oxygen sites. The only site that supported refinement is the one shown in figure 2 that resulted in a χ^2 value of 3.98 upon optimization of all parameters. This gives a structure with four Mo and four O atoms in a unit cell with five times the bulk 1×1 area, hence a model oxygen coverage of 4/5 or 0.8 ML. This agrees with the best determination of O coverage by Auger spectroscopy which gave a value of 0.66–0.8 ML with the brightest LEED pattern at 0.8 ML [8]. Other studies claim 0.72–0.86 ML [9] and 0.45–0.83 ML [10].

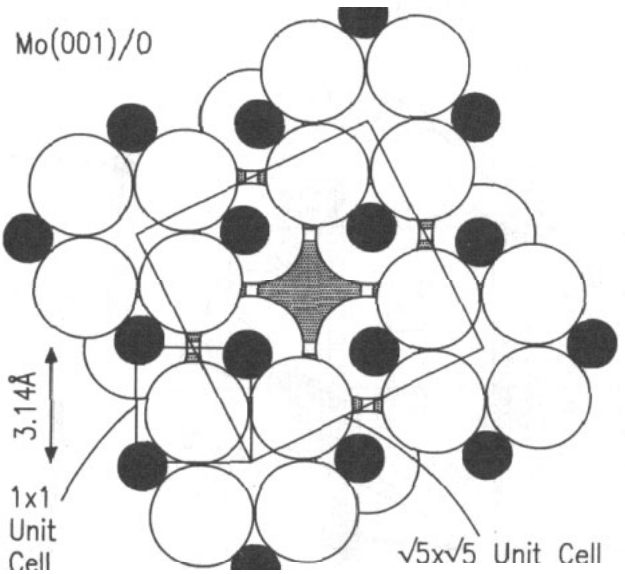

Figure 2. Top view of the atomic model derived here for the Mo(001)/O $\sqrt{5}\times\sqrt{5}$ structure. One top-layer Mo atom per unit cell (box) is missing; four O atoms line the corner of the vacancy that is created. The O atoms are bonded to two Mo atoms in the surface plane (bonds indicated) and one Mo in the layer below.

Figure 2 also shows the registry of the structure with respect to the bulk crystal below. This was determined using the integer-order data in the structure factor calculation. The integer-orders include the amplitude and phase information of the terminated bulk, so give strong interference with the surface structure factor components [20]. One parameter was adjusted here, the 'surface fraction', which represents the fraction of the surface that is reconstructed, assuming the rest to be disordered or simple 1×1. The surface fraction here was 93 ± 2%. The agreement between calculated and observed data is illustrated in figure 3.

Second-layer displacements are widely present in surface structures, and are a particularly important component of the clean reconstructed W(001) surface [21]. While it is possible to detect second-layer displacements with in-plane data [22], this important question is best answered with the out-of-plane data shown in figure 4. A relatively wide range of perpendicular momentum transfer is covered, but only a very gentle downward trend is observed for all the structure factors considered. This strongly suggests a single layer structure, a fact that is confirmed by simultaneous refinement of all data (figures 3 and 4) with a 3D model. This led to a final χ^2 value

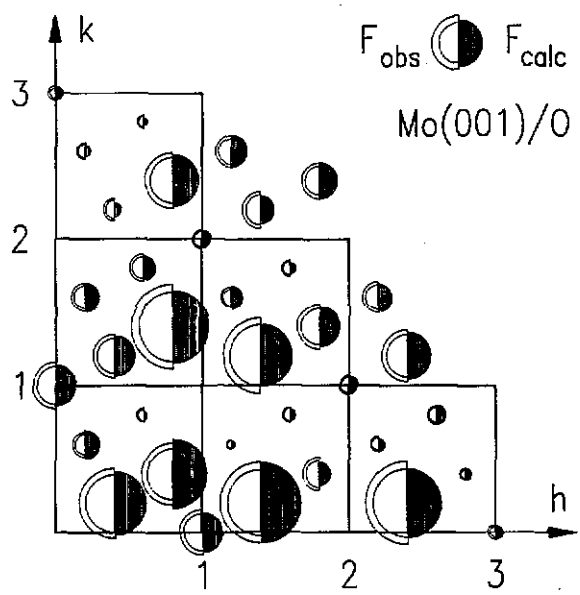

Figure 3. Comparison of observed and calculated structure factors for the model shown in figure 2. The radii of the unshaded half-circles are proportional to the observed amplitude at either extreme of the error bar; the shaded half-circle is the calculated value. The grid indicates the size of the bulk reciprocal lattice. The circles are positioned in the correct reciprocal space position for one of the twin domains; the other domain is omitted for clarity, but can be generated by reflection in one of the principal axes.

of 1.62 and gave the parameters in table 1 and the calculated curves in figure 4. The second-layer Mo displacements are insignificant at the 2σ level, where $\sigma = 0.004$ Å.

Table 1. Final structural parameters for the Mo(001)/O $\sqrt{5}\times\sqrt{5}$ structure. The x- and y-coordinates of the atomic positions are given as fractions of the $\sqrt{5}\times\sqrt{5}$ unit cell, which has an edge length of 7.02 Å. Each atom appears four times in the unit cell at positions obtained by fourfold rotation about the origin. Mo_1 and Mo_2 denote first- and second-layer atoms respectively; there is a fifth atom in the second layer at (0,0). The parameter errors obtained by least-squares fitting are given in parentheses.

Atom	x-coordinate	y-coordinate	Debye–Waller factor (Å^2)
Mo_1	0.2673(4)	0.1030(4)	3.36(23)
O	0.1722(27)	0.3880(25)	0.10(57)
Mo_2	0.2006(7)	0.3988(6)	—

There are two independent Mo–O bond lengths in the surface plane. Their refined values are 2.12 ± 0.02 Å and 2.12 ± 0.02 Å from table 1. These values fall in the middle of the range of values seen for bulk Mo oxides [1]. Figure 2 shows that there is a third bond from the O to the layer below. Unfortunately our technique is very insensitive to this length: because there are no second-layer Mo displacements, the out-of-plane data vary only *quadratically* with the relative heights of the top-layer Mo and O atoms. The dashed and dotted curves in figure 4 were calculated for vertical O displacements of 0.5 Å and 1 Å respectively, independent of the sign of

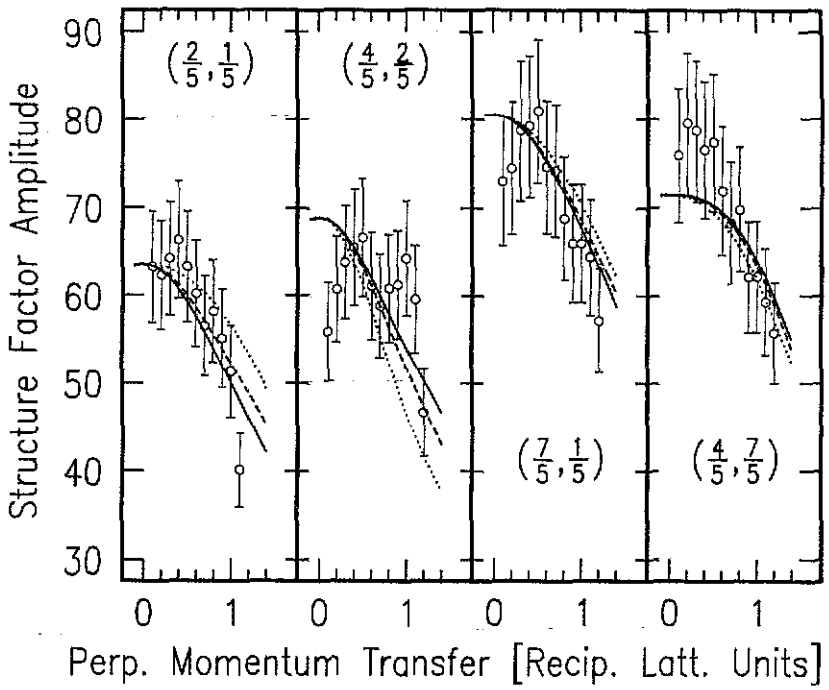

Figure 4. Out-of-plane measurements for the labelled reflections. The solid curve passing through the points is calculated from the model of figure 2. The dashed and dotted curves show the effect of displacing the plane of oxygen atoms by 0.5 Å and 1.0 Å, respectively. The curves are the same for displacements above or below the plane of the Mo atoms.

the displacement. The best fit is with no relative displacement, but the χ^2 value only rises by 0.4 at the extremes, indicating an uncertainty bigger than 1 Å. Thus we can merely conclude that the third Mo–O bond is 1.6 ± 1 Å. The choice of a threefold site would suggest three equal bonds (of 2.12 Å), and this is consistent with our error estimate. The site is shown in an oblique view in figure 5.

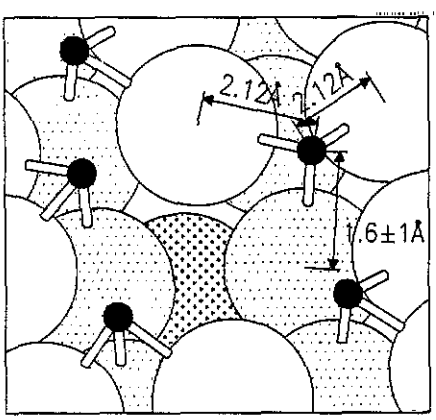

Figure 5. Oblique view of the environment of the surface oxygen atoms showing the bond lengths to each of the three Mo neighbours. The view is centred on the vacancy which is surrounded by O atoms (see figure 2). The oxygen atoms are solid, while the top layer Mo atoms are clear, the second layer lightly shaded and the third layer heavily shaded.

The structure (figure 2) can be viewed as a close-packed array of square clusters, each containing a core of four Mo atoms and four O atoms decorating the edges.

The Mo–Mo bond length is 2.851 ± 0.005 Å, which is 4.6% longer than the bulk bond length (2.725 Å), but 9.4% shorter than the separation of these atoms in an unreconstructed 1×1 surface (3.147 Å). This appears to be a compromise between close-packing and the desire to conserve the positions of the BCC lattice; the distortion from the BCC site is itself energetically unfavourable but the gain of two partially bonded neighbours balances this. It is interesting to note that the W–W bond length on the clean W(001) surface [21] (2.84 Å) is also 3.8% longer than in the bulk, and the coordination argument is analogous.

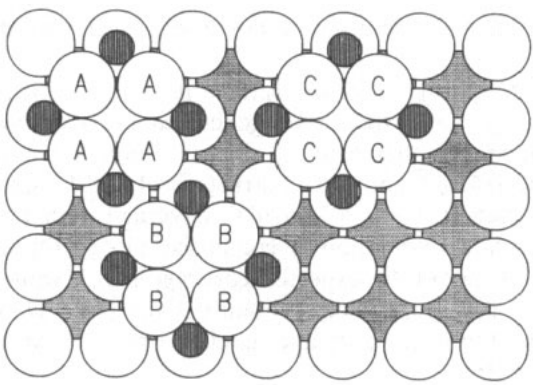

Figure 6. Possible packing arrangements of Mo_4O_4 clusters on an unreconstructed Mo(001) plane. If the plane is filled with clusters with relative positions A and B, the $\sqrt{5}\times\sqrt{5}$ structure (figure 2) is generated, which has the highest packing density, but lower $p4$ symmetry. Relative positions B and C would lead to a $p4m$ symmetric 'c(4×4)' structure with lower density. A 3×3 structure of still lower density is obtained by repetition of the AC packing.

This Mo_4O_4 cluster is apparently the elementary building block of the $\sqrt{5}\times\sqrt{5}$ structure. The closest non-overlapping packing of these is the $\sqrt{5}\times\sqrt{5}$ arrangement as figure 6 shows. Isolated clusters would align themselves with the substrate mirror planes (as shown in figure 6), but when they pack together into the $\sqrt{5}\times\sqrt{5}$ cell which has no mirror symmetry, they are free to rotate. They rotate by 5.5° in the direction favouring contact between the Mo of one cluster and the neighbouring cluster's O, thus improving the packing by partial bond formation. The rotation leads to a structure with no mirror symmetry, reminiscent of the $p4g$ structure of N/Ni(100) [13], but different because of the Mo vacancy. Even though the two in-plane Mo–O bonds are within error of the same length, the O site is still an asymmetric threefold because the bond angles are unequal.

In the case of the clean $\sqrt{2}\times\sqrt{2}$ reconstructed W(001) surface, the building block is a zig-zag chain of bonded W atoms. When chains pack together the interaction is mediated by a significant second layer displacement with 44% of the magnitude of the top layer [21]; there is no direct contact between the chains. Here for Mo(001)/O the situation is reversed: instead of the second layer displacement there is a direct attractive interaction between the Mo of one cluster and the O of the next (see figure 6), as manifested in the 5.5° rotation. The distance of 2.47 Å is nevertheless too long to be considered to be a fourth Mo–O bond.

The packing of the plus-shaped Mo_4O_4 clusters is not plane-filling and leaves one vacant site per $\sqrt{5}\times\sqrt{5}$ cell. This vacancy exposes a third-layer substrate atom

(shaded in figure 2). The temperature of formation of this structure must therefore be sufficient for lateral diffusion of vacancies to step edges to occur, so that an ordered 2D crystal can form. The $\sqrt{5}\times\sqrt{5}$ phase is not produced at room temperature, also suggesting Mo diffusion is important in its formation. Along the oxidation pathway referred to in the introduction, the vacancy formation may be a critical step towards oxygen-induced facetting of Mo(001). The decoration of the vacancy edges with O atoms lying in the plane of the top layer is analogous to the lining of missing rows in Cu(100)/O [12] and Cu(110)/O [11], and may play a similar role in the oxidation pathway of copper. It is noteworthy that an O–Mo bondlength of 2.12 Å implies that O could occupy interstitial (I) sites within the BCC Mo lattice, with its I–Mo distance of 2.22 Å, provided 6-coordination could be tolerated around O; the situation is very similar in FCC Cu [12].

The description of the Mo(001)/O $\sqrt{5}\times\sqrt{5}$ surface in terms of Mo_4O_4 clusters in figure 6 allows other plausible structures to be generated by changing the packing. The figure suggests arrangements that lead to a $p4m$ symmetric c(4×4) structure with lower density than the $\sqrt{5}\times\sqrt{5}$ and a 3×3 structure of still lower density. Since a c(4×4) structure is observed in LEED at lower O coverage than the $\sqrt{5}\times\sqrt{5}$ [8–10], it is tempting to speculate that it too is composed of Mo_4O_4 clusters in the manner indicated. From this model the expected coverage is 0.5, while the observed ranges are 0.2–0.65 (best at 0.4) [8], 0.2–0.5 [9] and 0.3–0.4 [10]. While this can be considered good agreement, the lower coverages could correspond to disorder in the form of further missing clusters.

In conclusion, we have identified the atomic structure of the Mo(001)/O $\sqrt{5}\times\sqrt{5}$ surface to be a vacancy model. It is a new type of adsorbate-induced reconstruction in which the top metal layer is pinched together into clusters. These covalently bonded Mo_4O_4 clusters overlap sufficiently to give rise to a 5.5° rotation. The O binding site is an unusual asymmetric threefold hollow site on the edge of each cluster. An alternative, lower density packing of clusters is a prediction of the structure of the lower coverage c(4×4) phase, that will be investigated in a future experiment.

Acknowledgment

NSLS is supported by the US Department of Energy under grant DE-AC012-76CH00016. D-MS acknowledges an Otto-Hahn fellowship from the Max-Planck-Gesellschaft, Federal Republic of Germany.

Appendix. Out-of-plane area and polarization corrections in the five-circle diffraction geometry

Figure A1 shows the scattering geometry. An incident beam of height h_1 and width w_1 strikes the sample with an incidence angle β. The diffracted beam is detected at a compound angle set by the five-circle diffractometer [19]: the in-plane angle is the conventional 2θ, while the out-of-plane component is denoted as α, as shown. The detector slit has dimension w_2 in-plane.

Normally the slit settings are chosen so that the active region of the sample, the parallelogram of intersection of the two beams of widths w_1 and w_2, stays within the boundary of the sample. The height of the beam h_1 is sufficient to illuminate

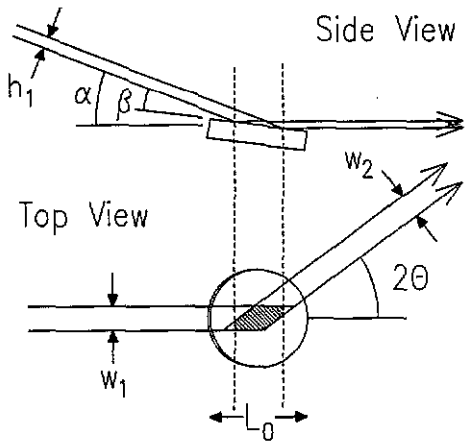

Figure A1. Five-circle diffraction geometry for surfaces. The angles and dimensions refer to the quantities used to derive the out-of-plane area and polarization corrections.

this entire region. The diffracted intensity is then proportional to the area of the parallelogram [18],

$$A_1 = w_1 w_2 / \sin 2\theta. \tag{1}$$

The measured intensities are therefore divided by the factor A_1 for proper normalization.

This becomes inadequate in two situations that must be accounted for in modifications to the area correction:

(i) when 2θ is very small and the active region runs off the edges of the sample, which is assumed to have length L_0 along the incident beam;

(ii) when the grazing incidence angle β is sufficiently large that the active region is incompletely illuminated. This is the situation shown in figure A1. A large β is commonly used in settings for large momentum transfer in the Fuoss–Robinson style surface diffractometer [14] because it helps to minimise the diffractometer χ angle that would otherwise distort the vacuum coupling bellows.

In this case the *effective* footprint length L of the beam on the sample is given by,

$$L = \min(L_0, L_1, h_1 / \sin\beta) \tag{2}$$

where L_1 is the length along the incident beam of the parallelogram defined by the in-plane slits,

$$L_1 = w_1 / \tan 2\theta + w_2 / \sin 2\theta. \tag{3}$$

The true active area is then given by,

$$A_2 = A_1 - \tfrac{1}{4}(L - L_1)^2 \tan 2\theta. \tag{4}$$

The measured intensities are then divided by the factor A_2 for proper normalization instead.

The out-of-plane detector also gives rise to a polarization correction. Synchrotron radiation is highly polarized in the horizontal plane and will lead to a cosine squared intensity fall-off with the component of the scattering angle that is in that plane. Normally the 2θ axis is horizontal when synchrotron radiation is used, and no correction is needed. However the angle α is about a vertical axis which requires a correction factor,

$$P = \cos^2(\alpha \cos 2\theta). \tag{5}$$

The measured intensities are divided by this factor P for proper normalization.

References

[1] Wells A F 1985 *Structural Inorganic Chemistry* (Oxford: Oxford University Press)
Wyckoff 1964 *Crystal Structures* vol 2 (New York: Wiley)
[2] Hayek K, Farnsworth H E and Park R L 1968 *Surf. Sci* **10** 429
[3] Kan H K A and Feuerstein S 1969 *J. Chem. Phys.* **50** 3818
[4] Dooley G W III and Haas T W 1970 *J. Chem. Phys.* **52** 461
[5] Tabor D and Wilson J M 1971 *J. Crystal Growth* **9** 60
[6] Riwan R, Guillot C and Paigne J 1975 *Surf. Sci.* **47** 183
[7] Kennett H M and Lee A E 1975 *Surf. Sci.* **48** 606
[8] Bauer E and Poppa H 1979 *Surf. Sci.* **88** 31
[9] Ko E I and Madix R J 1981 *Surf. Sci.* **109** 221
[10] Zhang C, van Hove M A and Somorjai G A 1985 *Surf. Sci.* **149** 326
[11] Feidenhans'l R, Grey F, Johnson R L, Mochrie S G J, Bohr J and Nielsen M 1990 *Phys. Rev.* B **41** 5420
[12] Zeng H C, McFarlane R A and Mitchell 1989 *Surf. Sci.* **208** L7
Wuttig M, Franchy R and Ibach H 1989 *Surf. Sci.* **213** 103
Robinson I K, Vleig E and Ferrer S 1990 *Phys. Rev.* B **42** 6954
[13] Wenzel L, Arvantis D, Daum W, Rotermund H H, Stöhr J, Baberschke K and Ibach H 1987 *Phys. Rev.* B **36** 7689
[14] Fuoss P H and Robinson I K 1984 *Nucl. Instrum. Methods* **222** 171
[15] Metal Crystals and Oxides Limited, Cambridge, UK
[16] Hulpke E and Smilgies D-M 1991 *Phys. Rev.* B **42** 1260
[17] Musket R J *et al* 1982 *Appl. Surf. Sci.* **10** 143
[18] Robinson I K 1990 *Handbook on Synchrotron Radiation* vol III ed D E Moncton and G S Brown (Amsterdam: Elsevier, North-Holland)
[19] Vlieg E, van der Veen J R, Macdonald J E and Miller M 1987 *J. Appl. Crystallogr.* **20** 330
[20] Feidenhans'l R, Nielsen M, Grey F, Johnson R L and Robinson I K 1987 *Surf. Sci.* **186** 499
[21] Altman M S, Estrup P J and Robinson I K 1988 *Phys. Rev.* B **38** 5211
[22] Robinson I K, Bohr J, Feidenhans'l R, Nielsen M, Grey F and Johnson R L 1989 *Surf. Sci.* **217** L435